Heat capacity of the two-dimensional electron gas in $GaAs/Al_xGa_{1-x}As$ multiple-quantum-well structures

J. K. Wang
Department of Physics, Princeton University, Princeton, New Jersey 08544

J. H. Campbell and D. C. Tsui
Department of Electrical Engineering, Princeton University, Princeton, New Jersey 08544

A. Y. Cho
AT&T Bell Laboratories, Murray Hill, New Jersey 07974

(Received 29 February 1988)

We apply the technique of ac calorimetry to a study of the heat capacity of the two-dimensional electron gas (2D EG) in $GaAs/Al_xGa_{1-x}As$ multiple-quantum-well structures. Below 2.3 K, we observe the 2D EG contribution to the sample heat capacity, in sweeps of magnetic field B, as oscillations of relative size 0.1%–0.2% periodic in $1/B$. The line shape of the oscillations is analyzed with reference to results calculated from theoretical models of the 2D EG density of states (DOS). We find that our experimental line shape is best fitted with a model DOS in which the broadening of the Landau levels oscillates as a function of B. The broadening attains maxima at B such that the heat capacity is at minima. This conclusion is in agreement with recent results from cyclotron-resonance experiments.

I. INTRODUCTION

In the past decade there has been much interest in the physical properties of two-dimensional electron-gas (2D EG) systems in a magnetic field B. If B is applied perpendicularly to the plane of the 2D EG, then the quantum-mechanical electron states exist only for discrete eigenenergies.[1] These Landau-level energies are of the form $(n+\frac{1}{2})\hbar\omega$, where n is a non-negative integer, and

$$\hbar\omega = e\hbar B/m_{2D} \tag{1}$$

is the cyclotron energy, defined in terms of B and the effective mass m_{2D} of the 2D EG. The orbital degeneracy per level, as well as the energy separation between Landau levels, depends linearly on B. Thus, the Landau-level filling factor $\nu = n_{2D}h/eB$, which is the number of levels occupied by a 2D EG with areal density n_{2D}, varies as $1/B$.

Disorder inevitably modifies the properties of a real 2D EG. Random scattering due to impurities, for example, will perturb the eigenenergies. The density of states (DOS), from which the macroscopic thermal and electronic properties of the 2D EG are determined, is accordingly perturbed from the ideal. In a perpendicular B, the DOS of the 2D EG will consist of a series not of ideal δ functions, but of broadened peaks centered at the discrete Landau-level energies. If the size of the spin-splitting energy is much smaller than the broadening width, then each peak is doubly degenerate and, at low temperatures, odd integral ν correspond to filling half of the uppermost occupied Landau level. The Fermi energy (E_F) will tend to lie within the width of one Landau level over small intervals of B. When the filling factor is nearly equal to an even integer, however, E_F moves from one Landau-level energy to an adjacent one across the energy gap between them. If B is ramped, E_F will move through successive Landau levels and interlevel gaps, and the DOS at E_F will undergo corresponding oscillations. The macroscopic properties of the 2D EG will exhibit $(1/B)$-periodic oscillations whose line shape depends on the detailed broadening of the Landau-level peaks in the DOS.[2–8]

Perhaps the $(1/B)$-oscillatory phenomenon that is most striking and best studied in the $GaAs/Al_xGa_{1-x}As$ 2D EG is the integral quantized Hall effect (IQHE) observed in measurements of the magnetoresistance tensor components.[3] The IQHE is closely associated with the localization of the states in each Landau level,[2,3] but such transport properties as electrical resistance depend primarily on the density of extended states alone. The total DOS can only be observed in such equilibrium thermodynamic properties as heat capacity and magnetization, which depend equally upon the contributions of localized and extended 2D EG states.[4–6]

In the past few years there has been some study of the heat capacity of the 2D EG (C_{2D}). Theoretical calculations have been performed by Zawadski and Lassnig using a model DOS with level broadening independent of B.[4] Gornik *et al.* have presented heat-pulse data[5] which reflect the "downward-cusp" shape of their calculated magnetooscillations in heat capacity.

In this paper, we present a study of the thermal properties of the 2D EG in a $GaAs/Al_xGa_{1-x}As$ multiple-quantum-well structure (MQWS). The B dependence of our sample heat capacity is found to differ qualitatively from that presented in Ref. 5. Our data cannot be fitted at all by assuming B-independent level broadening. The search for an adequate fit leads us to conclude that the

level width oscillates with the variation of B. The level width is found to be larger when E_F lies between Landau levels than when it coincides with a Landau level; the difference in widths increases at higher B, i.e., for smaller ν. This is in agreement with more recent theoretical and experimental work on Landau-level widths which supports a model in which screening of the scattering potential and the energy-level broadening influence each other self-consistently.[9–16]

In Sec. II we describe the principle of steady-state ac calorimetry. This technique was developed for and is commonly applied to systems with small heat capacities which are difficult to thermally isolate, and which exhibit small signal-to-background variations.[17,18] Sample preparation is described in Sec. III; experimental procedure and systematic checks are described in Sec. IV. The technique of ac calorimetry allows the accurate determination of internal (within the sample) and external (sample to holder and bath) relaxation times. Internal relaxation times are not generally found to be negligible. The apparent sample heat capacity could thus vary depending on the frequency or time scale of measurement if that scale is arbitrarily set. Heat-capacity data are taken in the correct frequency regime. In Sec. V we present the results from our study of the sample heat capacity as a function of B and temperature T. The data are analyzed in Sec. VI, and some conclusions are drawn about the form of the 2D EG DOS in Sec. VII.

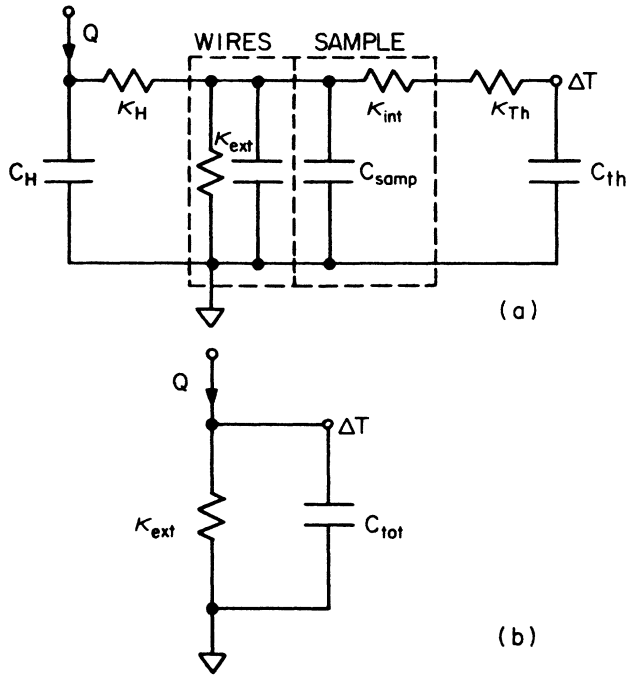

FIG. 1. Equivalent thermal circuits used in analysis of experimental frequency response: (a) with bulk thermal properties of sample and wires depicted as idealized discrete components within dashed borders; (b) simplified by assumption of Eqs. (4) and (6).

II. EXPERIMENTAL METHOD

In the ac-calorimetry technique the sample heater is driven by a sinusoidal voltage. If heater voltage $v_H(t) = \sqrt{2}V_H\cos(\omega t/2)$, using root-mean-square (rms) quantities, then the heat flux into the sample

$$\frac{dQ}{dt} = V_H^2(1+\cos\omega t)/R_H = P_H(1+\cos\omega t)\ , \tag{2}$$

where $P_H = V_H^2/R_H$. In steady state the constant component of heat flux will dissipate out the wires. Assuming that heat and T variations are small and linearizable, this will raise the sample T by an amount

$$\Delta T_{dc} = P_H/\kappa_{ext}\ , \tag{3}$$

where κ_{ext} is the thermal conductance from sample to holder and/or bath. The approximation that ΔT_{dc} is constant throughout the sample requires that

$$\kappa_{ext} \ll \kappa_{int}\ , \tag{4}$$

where κ_{int} is the thermal conductance across the thickness of the sample. That is, the T gradient across the sample is assumed to be negligible compared to that from sample to holder or bath. Equation (4) will be shown to be valid in the experiment itself.

To study heat capacity, we consider the ac component of heat flux. This induces temperature oscillations dependent on sample thermal properties which can be measured at *twice* the heater voltage frequency. For a real sample the amplitude of the ac temperature oscillations at the thermometer may be attenuated by the thermal relaxation rates between various parts of the sample and addenda.[17,18] The sample configuration can largely be analyzed as a discretized thermal circuit [see Fig. 1(a)]. In this model, Q denotes heat "charge," dQ/dt denotes heat flux, and C_i and κ_i, heat capacity of and thermal conductance across system component i, are the linearized dependences between small Q and dQ/dt, respectively, and T. The subscripts H, th, and samp indicate the heater, thermometer, and sample material, respectively. Including a heat equation solution for "distributed" thermal properties of the sample itself, Sullivan[17] originally calculated that to lowest order,

$$[\Delta T_{ac}(\omega)]_{rms} = \frac{P_H}{\omega C_{tot}\sqrt{2}}\left[1+\frac{1}{(\omega\tau)^2}+\frac{2}{3}\frac{\tau_{int}}{\tau}+(\omega\tau')^2\right]^{-1/2}. \tag{5}$$

Here $\tau = C_{tot}/\kappa_{ext}$, $(\tau')^2 = (C_H/\kappa_H)^2 + (C_{th}/\kappa_{th})^2 + \tau_{int}^2/90$, and $\tau_{int} = C_{samp}/\kappa_{int}$. If we assume that Eq. (4) holds, then the term inside curly brackets is unity for a bounded range of ω. That is,

$$[\Delta T_{ac}(\omega)]_{rms} \simeq \frac{P_H}{\sqrt{2}\omega C_{tot}}$$

$$\text{for } \omega \text{ such that } \tau^{-1} \ll \omega \ll (\tau')^{-1}\ , \tag{6}$$

and the thermal impedance $\Delta T_{ac}/P_H$ is dominated by the

"reactance" of the sample $(\omega C_{\text{tot}})^{-1}$. For such ideal samples and addenda, $\Delta T_{\text{ac}}(\omega)$, as well as ΔT_{dc}, can easily be derived from the simplified circuit of Fig. 1(b). In physical terms the heat flux is cycled into the sample quickly enough that the temperature response is measured before the heat dissipates to the holder or bath (in time τ), but also slowly enough that the temperature response is uniform within the sample system (in time τ'). On a plot of $\log_{10}(\omega \Delta T_{\text{ac}})$ vs $\log_{10}\omega$, this regime in ω appears as a plateau bounded at frequencies τ^{-1} and $(\tau')^{-1}$ by slopes falling off asymptotically at 45° angles.

The heat capacity is, in effect, continuously available as the reciprocal of a steady-state ac voltage measured from a thermometer resistance or thermoelectric sensor. This voltage may be analyzed and recorded as a function of slowly varying parameters such as B or the average T. Even with low input powers and variations ΔT_{ac}, and particularly with small C_{tot}, the voltage may be averaged over many cycles for very high precision (0.01%). Admittedly, the absolute accuracy of the technique is rarely better than 10% due to necessarily large addenda contributions. Many spectacular experiments have nevertheless been performed in which small changes in heat capacity are studied at high resolution, e.g., in film growth and phase transitions.[17,18]

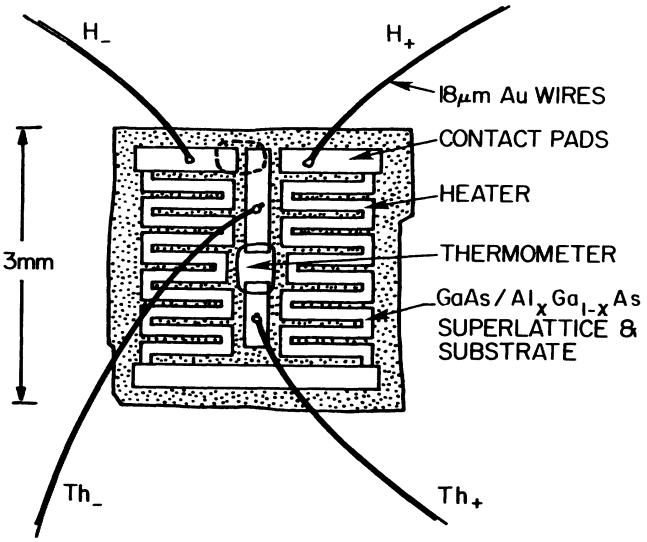

FIG. 2. Sample layout showing heater, thermometer, contact pads, and bonded wires (one pair each for heater and thermometer, $H_{\pm}$ and $Th_{\pm}$). In some samples, the contact pads of heater and thermometer grounds (H_- and Th_-) are connected through dashed region and wire Th_- is omitted.

III. SAMPLE PREPARATION

Samples were prepared from 75-period GaAs/$Al_xGa_{1-x}As$ MQWS material grown on semi-insulating GaAs wafers. The MQWS double layers alternated 175-Å GaAs and 460-Å $Al_xGa_{1-x}As$ thicknesses, with 60 Å of the $Al_xGa_{1-x}As$ modulation-doped ($n_D = 2\times10^{18}$ cm^{-3}) and distanced from adjacent GaAs layers by 200-Å $Al_xGa_{1-x}As$ space layers on each side. From transport measurements, we determined the 2D electron density $n_{2D} = (8.8\pm0.2)\times10^{11}$ electrons/cm^2 layer and the mobility $\mu = 100\,000$ cm^2/V s.

The substrate GaAs of 0.09-cm^2-area samples (6×10^{12} 2D electrons) was thinned by first hand-lapping and then acid-etching (in 4:1:1 volumetric ratio solution of sulfuric acid, hydrogen peroxide, and water at 70° C) to a thickness of $\sim$20 μm. A heater, a thermometer, and their contact pads were then evaporated onto the etched substrate side to avoid electrical coupling of thermal signal voltages to the 2D electrons (see Fig. 2). Finally, 17-μm-thick Au wires were attached to the contact pads by thermocompression bonding. At the lowest T studied (1.3 K) the wires and evaporated addenda were estimated to contribute as much as 40% of the total heat capacity of the system.

The heater film consisted of 250–400 Å gold (Au) evaporated atop a 60-Å-thick chromium (Cr) adhesive layer in a 100-square serpentine pattern with 250–400 Ω total resistance and covering $>60\%$ of sample area to ensure homogeneous heating of the sample. The Au-film resistance varied monotonically $<3\%$ in the ranges of T and B studied. The thermometer film was flash-evaporated 1000–2000 Å thick from gold-germanium alloy (Au_xGe_{1-x}, $x \simeq 0.1$) first treated through several cycles of baking and evaporating.[19,20] The resistance of the Au-Ge film closely followed a power-law dependence on T in the range studied, with $s = -d(\ln R)/d(\ln T)$ $\sim$0.6–1.0. In order to minimize spurious effects from thermal gradients across the sample, the thermometer was positioned in the center of the heater pattern with the gap between the films as narrow (<60 μm) as possible. On the ends of the heater and thermometer films 4000-Å-Au thick strips were evaporated to serve as the contact pads to which the Au wires were ball-bonded. The wires were then soldered to a commercial eight-pin header which was pressed into a socket carefully heat-sunk inside a resealable brass capsule. Thereby, the sample was at once (i) mechanically suspended and positioned, (ii) electrically connected to electronics, and (iii) thermally anchored to bath through a finite conductance.

IV. EXPERIMENTAL PROCEDURE

With the samples mounted inside, the brass capsule was indium-sealed, evacuated, and immersed in a liquid-helium bath. The sample holder T was measured with a carbon resistor calibrated over the range 1.2–4.3 K against the ^{4}He-bath vapor pressure using the T58 temperature scale.[21] The sample T was measured with the evaporated Au-Ge resistance thermometer itself calibrated against the holder T. In practice, a commercial dc current source converted the thermometer resistance to a voltage in a standard four-lead measurement. An audio-frequency oscillator with a ratio transformer served as a variable driving source for the sample heater. To measure ΔT_{ac}, the four-lead thermometer voltage was fed into a two-phase lock-in amplifier referenced to the

second harmonic ω of the heater voltage $\omega/2$. During sweeps of T or B, the lock-in-amplifier output was recorded digitally by a $5\frac{1}{2}$-digit digital multimeter (DMM) interfaced to a computer via a general purpose interface bus (GPIB) (see Fig. 3). The DMM sampling rate was once in 3 s or slower.

Various checks were routinely done at the beginning of each experimental run in order to ensure the consistency of thermal effects and the absence of spurious electrical effects. To avoid self-heating, the thermometer current was kept in the range 0.1–3 μA, where the current-voltage was linear. Over a reasonable range of heat voltage, the thermometer voltage amplitude at ω and the drop in the thermometer resistance were then each checked to be proportional to the square of the ac heater voltage amplitude at $\omega/2$. The drop in thermometer resistance corresponded to the rise in temperature ΔT_{dc} derived in Eq. (3). During experiments, the heater power amplitude was 0.3–12 μW, less being applied at lower T. For maximum total thermal signal, the thermometer current and the heat voltage were set at the highest values in the respective ranges given above.

sample size and geometry. Specifically, the addenda voltages, as applied along the etched substrate surface, could capacitively or conductively couple across the bulk lattice to the 2D EG. The applied or measured voltages would then shunt across and/or directly heat the 2D EG. Indeed, for samples with the addenda evaporated onto the thin cap layer ($\sim$3 μm thick) above the 2D EG, $(1/B)$-periodic oscillations were observed in the ac thermometer resistance. For samples with the addenda evaporated on the substrate side of the sample, no characteristic $(1/B)$-periodic oscillations were visible in the resistance of the addenda at a 0.05% level, whereas oscillations observed in thermal measurements at lowest T were at a 0.3% level. For a sample thickness of 20 μm and a heater area of 6 mm^2, the capacitance across the substrate presents a reactance $\sim$4500 MΩ/f, where $f=\omega/2\pi$ is the voltage driving frequency in Hz. Any B-dependent variations in electrical coupling to the 2D EG can shunt addenda resistances only in series with this substrate reactance. Then for a 300-Ω heater driven at 750 Hz, any shunting of the heater voltage is limited to a level of (300 Ω)/(6 MΩ), or $\lesssim$0.005%. The possibility of nonthermal coupling via the thermometer film can be similarly discounted. While the heater films cover more area susceptible to capacitive coupling with the 2D EG (6 mm^2 versus 0.1 mm^2), they also present proportionally less resistance (300 Ω versus 10 kΩ).

The above checks serve to establish that the lock-in–amplifier output (i.e., the signal voltage V_{sig}), measured at twice the heater frequency, purely represents a linearized temperature response to ac heating of the sample. As mentioned at the end of Sec. II, the product $\omega\Delta T_{ac}$ can be plotted versus ω to determine the bounded range in ω where ΔT_{ac} is simply proportional to C_{tot}^{-1}. In Figs. 4(a) and 4(b), plots taken for one sample show plateau regions at 1.3 and 4.6 K. Using a higher-range lock-in card set, we found this plateau, where Eq. (6) is valid, to extend over one decade in frequency at the lowest T studied. The plateau falloff at $\tau^{-1}=\kappa_{ext}/C_{tot}$ shifts to higher frequency at the lower T. This shift is expected for T above 1 K, where κ_{ext} due to the Au wires is linear in T, but C_{tot} is dominated by the T^3 dependence of the lattice. At still lower T this trend should slow down, as the T-linear electronic heat capacity of the 2D EG and the addenda begin to dominate C_{tot}.

After a proper operating ω was established at given T, C_{tot} was determined from Eq. (6). Given a set of values for P_H, ω, V_{sig}, and a temperature calibration for the thermometer voltage $V_{th}(T)$, one calculates that

$$C_{tot}(T;H=0)\equiv P_H/\sqrt{2}\omega[\Delta T_{ac}(\omega)]_{rms}$$
$$\text{where } [\Delta T_{ac}(\omega)]_{rms}=V_{sig}(dV_{th}/dT)^{-1}\ . \quad (7)$$

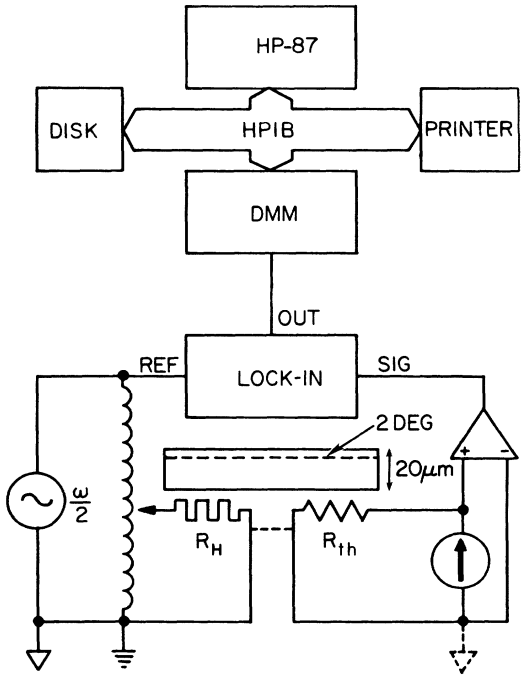

FIG. 3. Schematic of measurement electronics connected to sample.

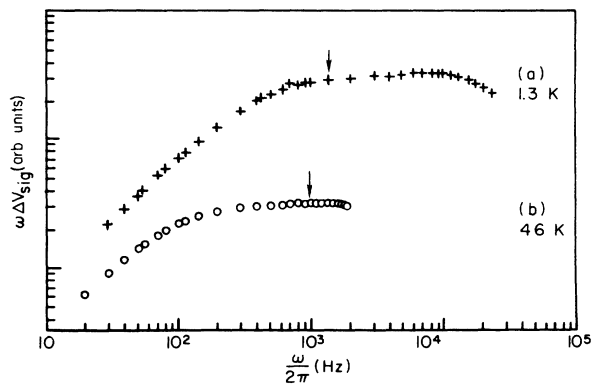

FIG. 4. Frequency response $\omega\Delta V_{sig}$ vs ω for a mounted sample at (a) 1.3 K (+) and (b) 4.6 K (○). Arrows indicate operating frequencies selected for measurements of C_{tot}.

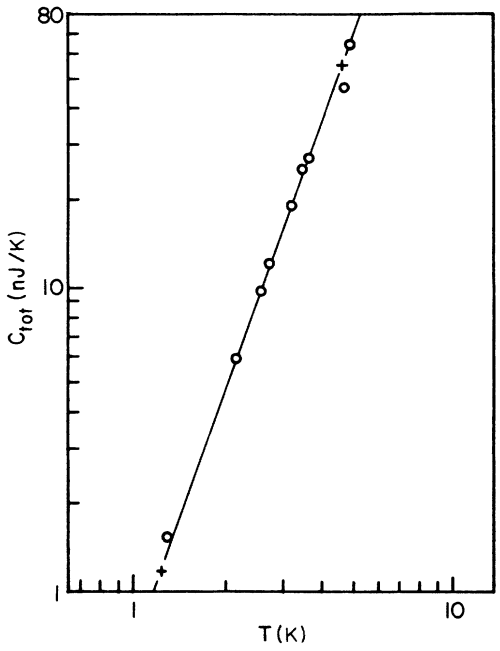

FIG. 5. C_{tot} (○) vs T. Reference line is drawn for comparison through values (+) calculated from Refs. 22–24 for the total heat capacity at 1.3 and 4.6 K contributed by the MQWS, substrate, Au wires, and evaporated addenda.

As an application of the technique, we plot the T dependence of C_{tot} obtained from our sample in Fig. 5. Using published thermal constants[22–24] and measured sample dimensions, we also calculated the total heat capacity expected for the MQWS and substrate, the Au wires, and the evaporated addenda. The values calculated at 1.3 and 4.6 K are plotted as + with a reference line drawn through them for comparison with the data (○). As expected, C_{tot} is dominated by the lattice substrate contribution proportional to T^3 in the temperature range studied. Only at 1.3 K, the lowest temperature examined, does the T-linear electronic contribution from the gold wires begin to be significant.

Above 1 K the lattice-dominated heat capacity of samples is expected to vary negligibly with B. Yet the signal voltage measured at ω in field sweeps varied as much as 60% from 0 to 8 T. At 4.2 K and above, this anomalous variation was due primarily to higher harmonic voltages superpositioned by the $\omega/2$ frequency heater voltage onto the thermometer voltage across their common ground. Unlike real signal voltage due to T variation at ω, this spurious contribution was dependent on the sign of the heater voltage relative to the thermometer voltage. Signal due only to heat capacity could therefore be isolated by averaging V_{sig} generated with forward and reversed current across the thermometer. At lower T, a fixed heater power includes larger thermometer voltage oscillations. The spurious thermometer voltage induced at ω by the heater is thus negligible below $\sim$2.5 K. But below 3 K, the relative thermometer magnetoresistance increased for some samples. C_{tot} was then necessarily determined from the T- and ω-dependence data at zero field. The contribution from C_{2D}, seen as $(1/B)$-periodic oscillations, could be analyzed as a small relative perturbation on a smooth background.

V. 2D EG HEAT CAPACITY VERSUS B AND T

In zero field the T-linear C_{2D} is estimated to contribute a maximum of 0.1% to C_{tot} at the lowest T studied.[24] This contribution is, by definition, not isolated in the measurement and thus not obtained in this experiment, but in sweeps of B the $(1/B)$-periodic oscillations observed in the signal voltage must be due entirely to the 2D EG, and the oscillatory line shape provides many interesting features for analysis. We routinely recorded field-sweep data, ramping B from 0 to 8–12 T in 12–20 min, though the range and the rate of ramping varied for some runs. At 2 K and below, small $1/B$ oscillations are visible in recorded field sweeps after subtraction of fits to background and magnification. We note that small relative variations in signal are closely approximated as negative changes in heat capacity, i.e.,

$$\Delta C_{tot}/C_{tot} \simeq -\Delta V_{sig}/V_{sig} \ . \tag{8}$$

The field sweeps were examined for $1/B$ oscillations by partially fitting the signal background for subtraction with a quadratic in B, so that

$$\Delta V_{sig} \simeq V_{sig} - (a_0 + a_1 B + a_2 B^2) \ , \tag{9}$$

ΔV_{sig} and V_{sig} are in μV, B is in T, and the constants a_0, a_1, and a_2 depend upon the heater voltage, thermometer current, and T. Prior to quantitative analysis of data, closer fits to signal background were computer-generated by a least-squares program in the form of fifth-order Chebyshev polynomials in B.[25]

Figure 6 shows the data at 4.6 K, with $\omega = 1$ kHz. Sample T was elevated above that of holder and bath (4.2 K at atmospheric pressure) by the constant term in Eq. (3). In order to enhance the signal-to-noise ratio, 20 sweeps were averaged by computer. The sweep average is shown without offset in Fig. 6(a). Oscillatory features are not visible in either the single sweeps or this average. They are also not resolved after magnification (50×) and the subtraction of a partial fit as in Eq. (9), with $a_0 = 11.155$, $a_1 = -0.125$, and $a_2 = 0.03$ [solid curve in Fig. 6(b)]. The complete computer-generated fifth-order polynomial fit (dashed curve) is plotted along with the partially fitted data. After subtraction of the complete fit, ΔV_{sig} is further magnified (250×) and inverted in Fig. 6(c) to represent ΔC_{tot}. It is evident that no oscillations can be assigned to the labeled even filling factors derived from the known n_{2D} and, in particular, the sharp spikes due to interlevel contributions at lower fields, as derived by Zawadzki and Lassnig,[4] are not observed. Based on the random noise fluctuations apparent in Fig. 6(c), an upper bound on the size of $1/B$ oscillations in C_{tot} at 4.6 K is $\sim$20 pJ/K, or $0.25 k_B$ per 2D electron.

The size of $1/B$ oscillations in C_{2D} is expected to de-

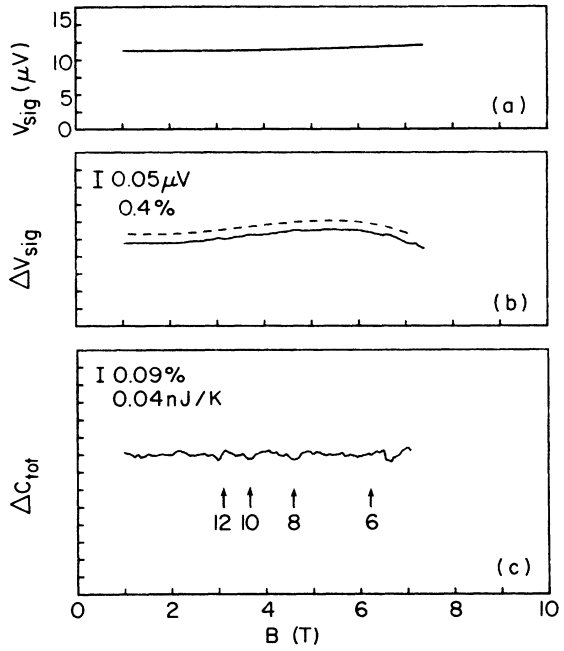

FIG. 6. Average of 20 sweeps of signal at 4.6 K with $\omega=1$ kHz: (a) without background subtraction; (b) after magnification (50×) and partial subtraction with Eq. (9) (solid curve). The computer-generated fifth-order polynomial fit (dashed curve) is shown for comparison. (c) The remainder after subtraction of this fit is plotted with further magnification (250×) and inversion. Numbers and arrows mark even filling factors. From Shubnikov–de Haas data, $n_{2D}=8.8\times10^{11}$ electrons/ cm^2/layer and $\mu=10^5$ cm^2/V s.

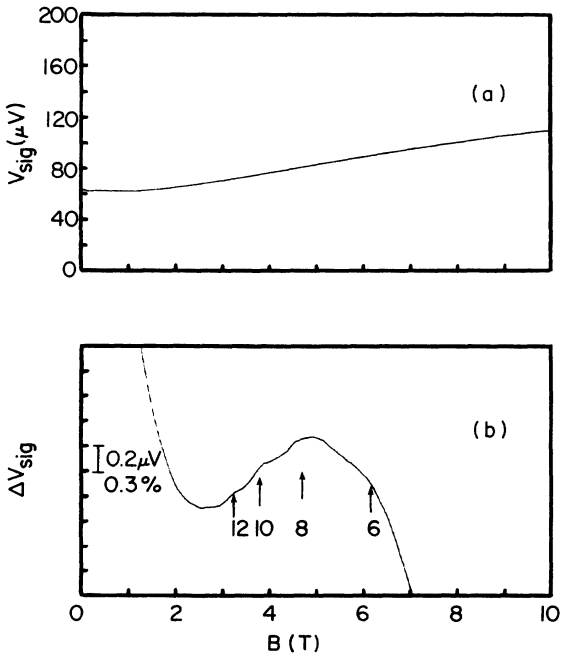

FIG. 7. Single sweep of signal at 1.7 K with $\omega=1$ kHz: (a) without background subtraction; (b) after partial subtraction with Eq. (9) and magnification (100×). Numbers and arrows mark even filling factors.

crease no faster than linearly with T,[4] whereas from Fig. 5 the lattice-dominated background heat capacity decreases at T^3. Consequently, the oscillations relative to the background are expected to be larger at lower T. At the same time, the noise of thermal origin is smaller at lower T. For example, at 4.6 K Johnson noise across the thermometer resistance is expected to contribute ~1 nV/$\sqrt{Hz}$ bandwidth. With a 4-s time-constant setting on measurements, the amplitude of this noise would correspond to 0.02% of total heat-capacity signal, or ~10 pJ/K at 4.6 K. This estimate is consistent with the experimental resolution of 20 pJ/K in Fig. 6(c). Across a thermometer resistance R, the size of Johnson noise relative to V_{sig} will depend on T as $(RkT)^{1/2}C_{tot}/(dR/dT)$ or, for $R\sim T^{-s}$ and $C_{tot}\sim T^3, T^{(s+9)/2}$. Since s is positive for Au-Ge, noise was expected to decrease faster than T^4. Indeed, at lower temperatures, $1/B$ oscillations were cleanly resolved above noise in single sweeps of field over a wide range in B.

In Fig. 7(a) data from a single field sweep at 1.7 K with $\omega=1$ kHz is shown unmagnified. While the thermometer displays pronounced magnetoresistance at 1.7 K and below, Eq. (8) correctly determines the amplitude of oscillations in heat capacity over small intervals of B. The partial fit in Eq. (9) was applied with $a_0=54.56$, $a_1=4.55$, and $a_2=0.17$. The remainder ΔV_{sig} is magnified (100×) and plotted in Fig. 7(b). Oscillations of $\sim0.1\%$ magnitude are visible with the $1/B$ periodicity expected for this 2D EG sample.

At the lowest T reached (1.3 K), ω was changed to 1.5 kHz. This was necessary to compensate for the relatively larger rate of thermal relaxation to holder or bath at low T, i.e., to stay on the frequency plateau in Fig. 4(a). Figure 8(a) shows that the $1/B$ oscillations are still not easily discernible in a field sweep of C_{tot}. But in Fig. 8(b) magnification (50×) and partial fitting with Eq. (9) ($a_0=282$, $a_1=45.5$, and $a_2=-1.80$) clearly resolves $1/B$ oscillations between 2 and 7 T. The computer fit to the background is plotted beneath as the dashed curve. After averaging of 22 sweeps, normalization with the computer fit, further magnification (1000×), and inversion ΔC_{2D} is shown in Fig. 8(c) to be a well-defined $1/B$ oscillatory waveform with 10 periods visible down to 1.5 T ($\nu=24$). At higher B, the waveform consists of peaks at Landau levels with smoothly curving valleys between. The peaks associated with the 2D EG appear to be superimposed on a longer period fluctuation, which is an artifact of our finite-order polynomial fit to the data.

We recorded sweeps of data at 1.3 K using heating frequencies ω spanning 0.1–8 kHz. At 200 Hz, $1/B$ oscillations were smaller, as is expected at lower ω off the plateau [Fig. 4(a)], where thermal relaxation out of the sample contributes additional apparent heat capacity. For ω in the interval 1.5–6.8 kHz on the plateau, no changes were observed in the shape or the relative size of the temperature oscillations. This is evidence that C_{2D} was measured with the heating frequencies used. Any frequency-dependent thermal inequilibrium between the 2D EG and the substrate should have appeared as variations with ω in the size and/or the shape of the $1/B$ oscillations. Above 6.8 kHz, $1/B$ oscillations were no longer visible.

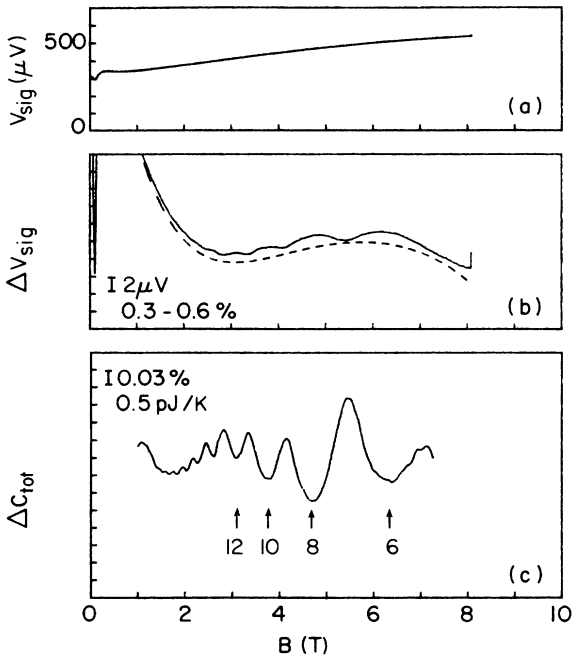

FIG. 8. Single sweep of signal at 1.3 K with $\omega=1.5$ kHz: (a) without background subtraction; (b) after magnification (50×) and partial subtraction with Eq. (9) (solid curve). The computer-generated fifth-order polynomial fit (dashed curve) is shown for comparison. (c) The remainder after subtraction of this fit is plotted with further magnification (1000×), averaging of 22 sweeps, and inversion. Numbers and arrows mark even filling factors.

The reciprocal of this frequency corresponds to an upper bound of ~ 22 μs on the 2D EG phonon relaxation time, but this bound may also represent an experimental high-frequency limit by the relaxation time between the substrate and addenda.

Samples were also prepared as described in Sec. III from a 15-period MQWS with $n_{2D}\sim 5\times 10^{11}$ electrons/cm^2 layer (total $n_{2D}\sim 7.5\times 10^{12}$ electrons/cm^2) and $\mu\sim 1.1\times 10^5$ cm^2/V s. Figure 9 shows a field sweep at 1.3 K with $\omega=1.6$ kHz that has been magnified after a partial fit using Eq. (9) with $a_0=406$, $a_1=26.7$, and $a_2=-2$. $1/B$ oscillations are discernible as labeled, but the smaller n_{2D} results in a smaller signal-to-background ratio. The qualitative line shape of the $1/B$ oscillations is similar for the two samples. Detailed analysis was therefore done only for data from the 75-period samples.

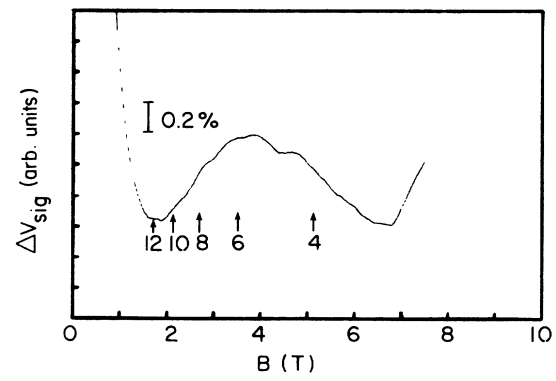

FIG. 9. Single sweep of signal for 15-period sample at 1.3 K with $\omega=1.6$ kHz, after magnification and partial subtraction with Eq. (9). Numbers and arrows mark even filling factors. From Shubnikov–de Haas data, $n_{2D}=5.5\times 10^{11}$ electrons/cm^2/layer and $\mu=1.1\times 10^5$ cm^2/V s.

VI. ANALYSIS AND DISCUSSION

It was noted in the preceding section that this experiment does not determine an accurate absolute value for C_{2D}. We measure the variation between minima and maxima in C_{2D}; C_{2D} at the minima is not distinguishable from the background, but the size and shape of the $1/B$ oscillations appearing atop the background can be quantitatively analyzed. The line shape of our data can be compared with results calculated from theoretical models,[4] and conclusions can be made about the 2D EG DOS. Because most of our field sweeps ramp up to 8 T, the largest and best-defined oscillation in heat capacity is associated with the $\nu=7$ filling factor. In this regime of B, spin splitting of the Landau levels is not detectable in the line shape of our data. Throughout the following analysis we assume the Landau levels to be doubly degenerate with no dependence on electron spin, so that E_F lies at the center of a Landau level for odd integer ν.

The 2D EG DOS is often modeled as the sum of contributions from Gaussian peaks with rms fullwidth Γ centered at each of the Landau levels.[4–6] We can crudely estimate Γ from

$$\Gamma=\hbar/\tau=e\hbar/m_{2D}=\sim 0.2 \text{ meV} \tag{10a}$$

using the electron-scattering time τ calculated from $\mu\sim 100\,000$ cm^2/V s. Another expression has been derived by Ando and Uemura.[26] They assume the level broadening to stem from scattering by a short-range impurity potential and obtain

$$\Gamma=2(e\hbar/m_{2D}c)(2B/\pi\mu)^{1/2}\sim 2 \text{ meV} . \tag{10b}$$

In this theory the DOS peaks at Landau levels are semielliptical, i.e., varying with energy as $\{1-2[(E-E_n)/\Gamma]^2\}^{1/2}$, where E_n is the nth Landau level as defined in the Introduction.

At arbitrary B, the electron states in the lowest Landau levels will be occupied at low T, filling levels up to E_F. The deviations from complete occupancy will be confined to within $\sim\pm kT$ of E_F. The B dependence of the DOS at E_F thus dominates that of C_{2D}. For low enough T, the heat-capacity of any degenerate Fermi gas is $\pi^2k^2T/3$ times the DOS at E_F.[24] An estimate of Γ can thus be derived from the amplitude of the heat-capacity oscillations. In the Gaussian model the DOS peaks are $(eB/\pi\hbar c\Gamma)(2/\pi)^{1/2}$.[5] At 1.3 K the oscillation amplitude at 5.3 T is ~ 3 pJ/K for our 75-period sample, implying that $\Gamma\sim 2$ meV at $\nu=7$. Strictly speaking, the oscillation amplitude measures the *difference* between the 2D EG heat capacity with E_F at a peak and with E_F between peaks. Since the DOS between Landau levels may not be

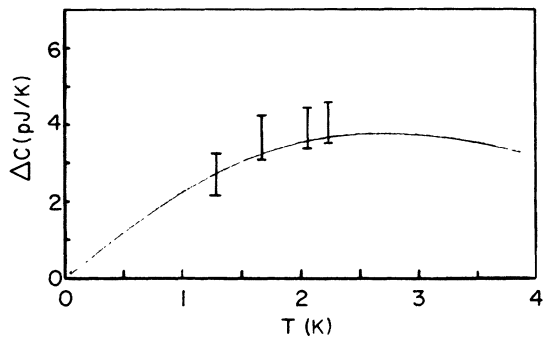

FIG. 10. Oscillation amplitude at $\nu=7$ (5.3 T) plotted vs T. Solid curve $C_{2D}(T)$ is calculated at the $\nu=7$ maximum relative to the $\nu=8$ (4.7 T) minimum, using $\Gamma(B)$ from Eq. (12).

negligible, Γ obtained here is only an upper bound.

In their calculations of the 2D EG heat capacity, Zawadzki and Lassnig[4] take Γ to be constant for all Landau levels and for all B. With the further restriction that $\hbar\omega \gg \Gamma$ and kT, they find a strict kT/Γ dependence. For our sample, when $\nu=7$ at 5.3 T, $\hbar\omega=9$ meV, much larger than kT in our experiments and the upper bound ~ 2 meV on Γ. Our measured heat capacity at $\nu=7$ can therefore be analyzed in terms of the calculations in Ref. 4. In Fig. 10 the points with error bars give the T dependence of our experimental peak-to-peak oscillation amplitude at $\nu=7$. A qualitative comparison with the calculations then allows a limit to be set on Γ within the model of Ref. 4. The calculated C_{2D} is maximum when $kT/\Gamma \sim 0.2$. Our data monotonically increases with T up to 2.3 K, which implies that $\Gamma > \sim 1.1$ meV. This conflicts with the value estimated from $\Gamma=\hbar/\tau \sim 0.2$ meV [Eq. (10a)], though not with $\Gamma \sim 2$ meV from the short-range scattering theory [Eq. (10b)].

For $\hbar\omega \gg \Gamma$ and kT, E_F and the associated region of incomplete occupancy of states will tend to lie within Γ of a Landau-level energy. The 2D EG DOS at E_F will vanish only as values of B are swept such that an integral number of levels is exactly filled and E_F jumps across the energy gap between adjacent levels. The oscillations in C_{2D} will therefore appear as broad domes separated by cusped minima [e.g., Fig. 11(a)]. Our data [Fig. 7(c)], on the other hand, exhibits smooth valleys between pointed peaks, so that over large intervals of B the DOS at E_F and thereby C_{2D} have values close to those at minima. We conclude that E_F passes smoothly between Landau levels, and the DOS between Landau levels is not negligible compared to the DOS at the Landau-level peaks.

The preceding qualitative analysis was further explored in numerical calculations following the approach of Ref. 4. For arbitrary B the DOS was approximated as a superposition of peaks centered at the Landau levels with a Gaussian distribution in energy. The Gaussian peaks are normalized so that the integrated DOS per level equals the degeneracy per level in the ideal 2D EG. As in Ref. 5, a constant-background DOS was incorporated as a hypothetical origin of the non-negligible DOS between levels. That is, the summation of Gaussian peaks could be normalized by $1-x$ and a fraction x of the total DOS added as a B-independent term. The calculated C_{2D} is

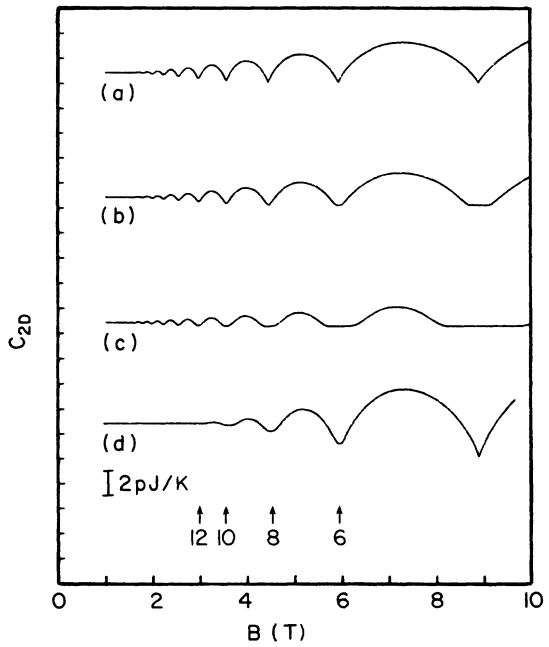

FIG. 11. $C_{2D}(B)$ calculated using various values for Γ, x, and T: (a) $\Gamma=2.5$ meV, $x=0$; (b) $\Gamma=2.5$ meV, $x=20\%$; (c) $\Gamma=2.0$ meV, $x=60\%$; (d) $\Gamma=4.4$ meV, $x=0$. $T=1.3$ K for plots (a)–(c); (d) is at 4.5 K. Numbers and arrows mark even filling factors.

shown as a function of B using various values of Γ and x in Fig. 11. With Γ and x held independent of B, the qualitative $(1/B)$-oscillation line shape remains the same with values of Γ as high as 4.4 meV. As is evident from Figs. 11(b) and 11(c), the assumption of as high as 60% constant-background DOS in calculations at 1.3 K merely modifies the cusped minima between Landau levels into flat interlevel regions of constant heat capacity (because the flat-background DOS dominates the behavior of the total DOS only at minima). The rounded minima and relatively sharp maxima in our experimental line shape cannot be fitted with the B-independent parameters Γ and x alone.

Recent measurements of the cyclotron-resonance (CR) linewidth have shown that Γ does vary with B.[9–11] As a function of ν or B, Γ oscillates, attaining maxima when E_F passes between adjacent Landau levels. To explain this, theoretical studies[12–16] have taken into account the self-consistent screening expected for the long-range impurity potentials arising from the doped $Al_xGa_{1-x}As$ layer in $GaAs/Al_xGa_{1-x}As$ heterostructures. When E_F coincides with a Landau level, the DOS at E_F is high and screening of impurity potentials is most effective. Consequently, the level is broadened little. Between Landau levels, however, relatively few electrons states exist at E_F for screening, and impurity scattering broadens level widths to greater extent. An oscillating level width results from self-consistent calculations of screening and level broadening, in agreement with the conclusions from the CR experiments. However, it has not been applied towards calculations of the B dependence of C_{2D}.

We have studied C_{2D} with the level width Γ varying periodically in $1/B$ in the Gaussian model. No constant

background of states is assumed. In Fig. 12(a) we show a plot of the B dependence of Γ:

$$\Gamma(B)=2.68/[1+(B^2/19)]^{1/2} + \{[1+(B^2/19)]^2-1\} \times\{1+\cos(\pi\nu)/[\cos^2(\pi\nu)]^{0.05}\}/2.5\ , \quad (11)$$

where B is in units of T, Γ is in units of meV, and ν is the dimensionless filling factor. The various functional components in Eq. (11) were fitted by matching to various features of the line shape of our data, including the ν dependence of the amplitude of $1/B$ oscillations and the "sharpness" of peaks. Consistent with the CR results cited above,[9,10] the maxima of Eq. (11) are at even integer values of ν, where E_F lies between levels. As labeled in Fig. 12(b), the lower curve shows the calculated C_{2D} at 1.3 K using Γ given by Eq. (11), and the upper curve is our experimental data from Fig. 8(c). It is evident that the data is well reproduced with $\Gamma(B)$ given by Eq. (11). The solid curve in Fig. (10) gives the T dependence of C_{2D} calculated at the $\nu=7$ (5.3 T) maximum relative to the $\nu=8$ (4.7 T) minimum, with the values of Γ determined from Eq. (11). Our measured T dependence at low T is consistent with the oscillatory Γ model.

The observed $1/B$ oscillations may not represent the total C_{2D}. That is, the line shape in Fig. 8(c) possibly represents $C_{2D}(B)$ minus a smooth, nonoscillatory term. The peak heights in the B dependence of the DOS and C_{2D} are proportional to Γ^{-1}. Therefore, if C_{2D} at a Landau level is actually greater than the observed size of the $1/B$ oscillation, then $\Gamma(B)$ should be smaller than the value given by Eq. (11), but any nonoscillatory term is expected to be no larger than C_{2D} at zero field, and the zero-field C_{2D} is much smaller than the size of oscillations above 3 T. At least in this range of B, $\Gamma(B)$ can differ only slightly from Eq. (11) and will exhibit the $(1/B)$-oscillatory features plotted in Fig. 12(a).

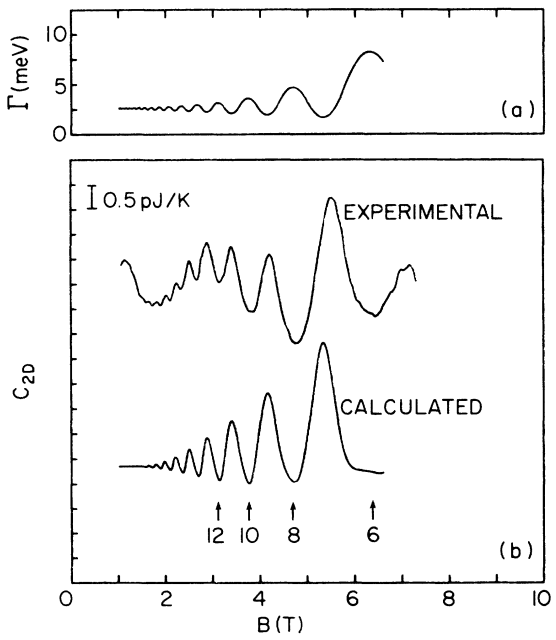

FIG. 12. (a) $\Gamma(B)$ from Eq. (11). (b) The corresponding $C_{2D}(B)$ (CALCULATED curve) at 1.3 K and Fig. 8(c) (EXPERIMENTAL curve) are plotted on the same scale for comparison. Numbers and arrows mark even filling factors.

As mentioned in Sec. I, studies of various other properties of the 2D EG have indicated the existence of a significant DOS between broadened Landau levels.[6,7] Eisenstein *et al.*,[6] for example, fitted their magnetization data for a GaAs/Al_xGa_{1-x}As 2D EG with a level width $\Gamma(B)\sim B^{1/2}$. As they point out, different aspects of the DOS dominate the line shape of the $1/B$ oscillations observed in different physical phenomena. For example, the maxima of oscillations appear in magnetization when E_F is between levels, whereas they appear in heat capacity when E_F is at the center of a level. Values for Γ estimated from the amplitudes measured for these two properties are therefore not directly comparable. But we note in passing that Eisenstein *et al.*[6] obtain a rms full width $\Gamma=4.4$ meV at 5 T for their sample. This value is in very close agreement with our fit to Γ, ~ 5 meV at 4.8 T when E_F lies between levels in our sample.

We cannot directly compare our data with those from an earlier experimental study of C_{2D} by Gornik *et al.*[5] In their report, they fit the B dependence of their specific-heat data by a model with $\Gamma=2.5$ meV and a constant-background DOS $x=15\%$ of the total DOS. While their value of Γ lies in the range covered by our fitting function $\Gamma(B)$, they find that their data is adequately fitted with both Γ and x independent of B. As we have shown from the calculations plotted in Fig. 11, a fit with constant Γ results in a line shape qualitatively different from that of our data. In our data, the maxima in B-field sweeps of heat capacity are distinctly sharper than the minima. In Ref. 5 the converse is true.

Another discrepancy is with regard to the interlevel peaks at higher T. As explained by Zawadzki and Lassnig,[4] the interlevel spikes are expected only at low B and high T. At 5 K, for example, $kT\sim 0.5$ meV, whereas the Landau-level spacing in the GaAs/Al_xGa_{1-x}As 2D EG system is 1.74 meV at $B=1$ T. Above 4 K, in a sample with similar physical parameters, Gornik *et al.*[5] observe interlevel spikes at low B (around 2 T) of size 0.03–5 % of C_{tot}. In an average of 30 field sweeps, from 0 to 5 T at 4.6 K, we observe no $1/B$ oscillations above the 0.03% level. In the calculated C_{2D} for 4.6 K using $\Gamma(B)$ given in Eq. (11), rounded interlevel maxima are of size less 0.5 pJ/K, or 0.001% of C_{tot}. Within experimental resolution, the absence of sharp interlevel spikes in our data is consistent with our model of a B-dependent level broadening. In a general system, peaks in heat capacity indicate that the energy of the system jumps sharply within a small range of T. In a 2D EG above 0 K, with E_F between Landau levels, this jump arises from a sharp increase of E_F with T across the interlevel energy gap and the corresponding sharp increase in the occupation of the higher level states. But if the energy gap is not completely devoid of states, then an infinitesimal increase in T results in an infinitesimal increase in the occupation of the interlevel states continuously distributed in energy above E_F. Interlevel spikes in heat capacity are then less sharp or even absent.

VII. CONCLUSION

We have presented a systematic study of the thermal properties of a GaAs/$Al_xGa_{1-x}As$ MQWS 2D EG based on the technique of ac calorimetry. After optimizing the limiting parameters of the system, we have studied the heat capacity and observed oscillations periodic in $1/B$. The dependence on T and ω of these oscillations are reported and analyzed. The T dependence and the oscillation amplitude at fixed low T are separately analyzed in order to set lower limits on the Landau-level width. In agreement with the results of various other experimental studies of the GaAs/$Al_xGa_{1-x}As$ 2D EG DOS, values obtained for level broadening at high B are much larger than derived from the zero-field mobility. The detailed line shape of the $1/B$ oscillations itself gives information regarding the form of the DOS. A form derived from fitting data is discussed with reference to the most recent calculations of level broadening in GaAs/$Al_xGa_{1-x}As$ heterostructures. Although the absolute value of C_{2D} is not measured in our experiment, its qualitative B dependence is shown to agree with other experimental work that Landau-level broadening oscillates strongly with $1/B$.

The qualitative line shape of our data differs markedly from that seen in the C_{2D} data reported in Ref. 5. The 2D EG density and mobility of at least one of their samples is similar to that of our material (7.7×10^{11} electrons/cm^2 and 80 000 cm^2/V s, respectively, for their sample 2). But they find their heat-capacity data to be adequately fitted by taking the DOS to consist of Gaussian peaks with both the level broadening and the background of states independent of B.

In seeking to explain this difference of line shape, it should be realized that the measured mobility does not reveal the relative contribution from various sources to the total screening with a given sample.[12] As explored in Refs. 11–16, the effect of impurity scattering on the 2D EG DOS may vary greatly, depending upon the relative proximity of the impurities to the 2D EG. In particular, the results of Ando and Murayama[14,15] indicate that the B dependence of Landau-level broadening is strongly dependent on spacer thickness. In view of the recent data reported by Eisenstein *et al.*[8] on the thermal conductance of GaAs/$Al_xGa_{1-x}As$ heterostructures, it may also be that the line shapes of data differ because the $1/B$ oscillations reported in Ref. 5 are not in heat capacity, but in 2D EG-phonon coupling. It is noted that the oscillatory shape in the dc thermal conductance data of Eisenstein *et al.*[8] is very similar to that observed in the heat-capacity data in Ref. 5, with extrema at even-integer filling factors sharper than at odd intergers. This possibility can be resolved only by a detailed experimental investigation of both phenomena in identical samples.

We note that we have presented a calorimetry technique in Sec. III designed specifically for measurement of steady-state heat capacity.[17,18] Our film patterns are positioned to minimize temperature gradients between. The frequency dependence of our thermal signal is empirically analyzed to establish the appropriate parameter range for study of heat capacity. Moreover, the nonequilibrium thermal properties of the 2D EG system can be systematically investigated through a modified ac-calorimetry technique. By using different sample geometries in studies of frequency or time dependence, the interplay between 2D EG heat capacity and coupling to phonons in thermal processes could be thoroughly elucidated. In the future, heat capacity should also be studied at lower (mK) temperatures, where the experimental signal resolution is potentially better and its theoretical dependence on the DOS is clearer. In view of recent significant progress in sample growth technology, it may also be feasible to obtain heat-capacity data for MQWS's of higher quality, i.e., with mobilities higher than 10^5 cm^2/V s. Future experiments along these lines will help to further our understanding of the 2D EG DOS in high magnetic field.

ACKNOWLEDGMENTS

The work at Princeton University is supported by the U.S. Office of Naval Research through Contract No. 00014-82-K0450, the U.S. National Science Foundation through Grant No. 82-12167, and grants from Siemens RTL and the NEC Corporation.

[1]The theoretical problem of an ideal, noninteracting 2D EG in a perpendicular magnetic field is completely solved. A derivation can be found in the Introduction, by R. E. Prange, to *The Quantum Hall Effect,* edited by R. E. Prange and S. M. Girvin (Springer-Verlag, New York, 1987).

[2]T. Ando, A. B. Fowler, and F. Stern, Rev. Mod. Phys. **54**, 437 (1982).

[3]D. C. Tsui and A. C. Gossard, Appl. Phys. Lett. **38**, 550 (1981).

[4]W. Zawadzki and R. Lassnig, Surf. Sci. **142**, 225 (1984); W. Zawadzki and R. Lassnig, Solid State Commun. **50**, 537 (1984).

[5]E. Gornik, R. Lassnig, G. Strasser, H. L. Störmer, A. C. Gossard, and W. Wiegmann, Phys. Rev. Lett. **54**, 1820 (1985); Surf. Sci. **170**, 277 (1986).

[6]J. P. Eisenstein, H. L. Störmer, V. Narayanamurti, A. Y. Cho, A. C. Gossard, and C. W. Tu, Phys. Rev. Lett. **55**, 875 (1985).

[7]T. P. Smith, B. B. Goldberg, P. J. Stiles, and M. Heiblum, Phys. Rev. B **32**, 2696 (1985).

[8]J. P. Eisenstein, A. C. Gossard, and V. Narayanamurti, in Proceedings of the Seventh International Conference on Electronic Properties of Two-Dimensional Electron Systems, Santa Fe, 1987 [Surf. Sci. (to be published)]; J. P. Eisenstein, A. C. Gossard, and V. Narayanamurti, Phys. Rev. Lett. **59**, 12 (1987).

[9]T. Englert, J. C. Mann, C. Uihlein, D. C. Tsui, A. C. Gossard, Solid State Commun. **44**, 1301 (1982).

[10]M. J. Chou, D. C. Tsui, and G. Weimann, Phys. Rev. B **37**, 848 (1988).

[11]W. Seidenbusch, E. Gornik, and G. Weimann, Phys. Rev. B **36**, 9155 (1987).

[12]S. Das Sarma, Phys. Rev. B **23**, 4592 (1981); S. Das Sarma and X. C. Xie, Phys. Rev. Lett. **61**, 738 (1988).

[13]R. Lassnig and E. Gornik, Solid State Commun. **47**, 959 (1983).
[14]T. Ando and Y. Murayama, J. Phys. Soc. Jpn. **54**, 1519 (1985).
[15]Y. Murayama and T. Ando, Phys. Rev. B **35**, 2252 (1987).
[16]W. Cai and C. S. Ting, Phys. Rev. B **33**, 3967 (1986).
[17]The technique was introduced in P. Sullivan and G. Seidel, Phys. Rev. **173**, 679 (1968). Subsequent applications in small sample calorimetry at low T are reviewed in I. Hatta and A. J. Ikushima, Jpn. J. Appl. Phys. **20**, 1995 (1981), as well as G. R. Stewart, Rev. Sci. Instrum. **54**, 1 (1983).
[18]J. H. Campbell and Michael Bretz, Phys. Rev. B **32**, 2861 (1985).
[19]B. W. Dodson, W. L. McMillan, J. M. Mochel, and R. C. Dynes, Phys. Rev. Lett. **46**, 46 (1981).
[20]M. Chinn (private communication).
[21]*The 1958 ^{4}He Scale of Tempeature,* Nat. Bur. Stand. (U.S.) Monograph No. 10 edited by F. G. Brickwedde (U.S. GPO, Washington, D.C., 1960).
[22]T. C. Cetas, C. R. Tilford, and C. A. Swenson, Phys. Rev. **174**, 835 (1968).
[23]*CRC Handbook of Chemistry and Physics,* 67th ed., edited by R. C. Weast, M. J. Astle, and W. H. Beyer (Chemical Rubber Co., Boca Raton, FL, 1986), pp. B93 and D94.
[24]N. W. Ashcroft and N. D. Mermin, *Solid State Physics* (Saunders College, Philadelphia, 1976), p. 46.
[25]Philip R. Bevington, *Data Reduction and Error Analysis for the Physical Sciences* (McGraw-Hill, New York, 1969), p. 172.
[26]T. Ando and Y. Uemura, J. Phys. Soc. Jpn. **36**, 959 (1974).